

1 | **Responses to the Editor:**

2
3
4
5
6
7
8
9
10
11
12
13
14
15
16
17
18
19
20
21
22
23
24
25
26
27
28
29
30

We thank the Editor again for his careful reading of the manuscript and helpful comments. We have revised the manuscript following the suggestions as is described below.

1. Please enhance the quality of the figures by increasing both the resolution and the sizes of the figure legends.

According to the Editor's suggestion, we re-plot the figures with better quality and large sizes of the figure legends.

2. The following studies are concerned with the impact of carbonaceous aerosol on air pollution that may be referred to in the introduction:
Jia R., M. Luo, Y. Liu, Q. Z. Zhu, S. Hua, C. Q. Wu and T. B. Shao, 2019: Anthropogenic Aerosol Pollution over the Eastern Slope of the Tibetan Plateau. *Advances in Atmospheric Sciences*, 2019, 36(8): 847-862.

Zhu Q., Y. Liu, R. Jia, S. Hua, T. Shao, B. Wang, 2018: A numerical simulation study on the impact of smoke aerosols from Russian forest fires on the air pollution over Asia. *Atmospheric Environment*, 182,263-274.

According to the Editor's suggestion, we have added these 2 references in the introduction and references.

31 **Ozone enhancement due to photo-disassociation of**
32 **nitrous acid in eastern China**

33
34 **Xuexi Tie^{1,2}, Xin Long^{1,5}, Guohui Li¹, Shuyu Zhao¹, Junji Cao¹, Jianming Xu^{3,4}**
35
36
37

38 ¹KLACP, SKLLQG, Institute of Earth Environment, Chinese Academy of Sciences, Xi'an 710061,
39 China

40
41 ²Center for Excellence in Urban Atmospheric Environment, Institute of Urban Environment, Chinese
42 Academy of Sciences, Xiamen 361021, China

43
44 ³Shanghai Meteorological Service, Shanghai, 200030, China

45
46 ⁴Shanghai Key Laboratory of Meteorology and Health, Shanghai, 200030, China

47
48 ⁵School of Environment Science and Engineering, Southern University of Science and Technology,
49 Shenzhen 518055, China

50
51
52 *Correspondence to:* XueXi Tie (tiexx@ieecas.cn) or
53 Jianming Xu (metxujm@163.cn)
54
55
56
57

58 **Abstract**

59 PM_{2.5}, a particulate matter with a diameter of 2.5 micrometers or less, is one of the
60 major components of the air pollution in eastern China. In the past few years, China's
61 government made strong efforts to reduce the PM_{2.5} pollutions. However, another
62 important pollutant (ozone) becomes an important problem in eastern China. Ozone
63 (O₃) is produced by photochemistry, which requires solar radiation for the formation
64 of O₃. Under heavy PM_{2.5} pollution, the solar radiation is often depressed, and the
65 photochemical production of O₃ is prohibited. This study shows that during late
66 spring and early fall in eastern China, under heavy PM_{2.5} pollutions, there were often
67 strong O₃ photochemical productions, causing a co-occurrence of high PM_{2.5} and O₃
68 concentrations. This co-occurrence of high PM_{2.5} and O₃ is un-usual and is the main
69 focus of this study. Recent measurements show that there were often high HONO
70 surface concentrations in major Chinese mega cities, especially during daytime, with
71 maximum concentrations ranging from 0.5 to 2 ppbv. It is also interesting to note that
72 the high HONO concentrations were occurred during high aerosol concentration
73 periods, suggesting that there were additional HONO surface sources in eastern China.
74 Under the high daytime HONO concentrations, HONO can be photo-dissociated to be
75 OH radicals, which enhance the photochemical production of O₃. In order to study the
76 above scientific issues, a radiative transfer model (TUV; Tropospheric
77 Ultraviolet-Visible) is used in this study, and a chemical steady state model is
78 established to calculate OH radical concentrations. The calculations show that by
79 including the OH production of the photo-dissociated of HONO, the calculated OH
80 concentrations are significantly higher than the values without including this
81 production. For example, by including HONO production, the maximum of OH
82 concentration under the high aerosol condition (AOD=2.5) is similar to the value
83 under low aerosol condition (AOD=0.25) in the no-HONO case. This result suggests
84 that even under the high aerosol condition, the chemical oxidizing process for O₃
85 production can occurred, which explain the co-occurrence of high PM_{2.5} and high O₃
86 in late spring and early fall seasons in eastern China. However, the O₃ concentrations
87 were not significantly affected by the appearance of HONO in winter. This study
88 shows that the seasonal variation of solar radiation plays important roles for
89 controlling the OH production in winter. Because the solar radiation is in a very low
90 level in winter, adding the photolysis of HONO has smaller effect in winter than in

91 other seasons, and OH remains low values by including the HONO production term.
92 This study provides some important scientific highlights to better understand the O₃
93 pollutions in eastern China.

94

95 **Keywords; High PM_{2.5} and O₃, eastern China, HONO photolysis**

96

97

98

99

100

101

102 1. Introduction

103

104 Currently, China is undergoing a rapid economic development, resulting in a higher
105 demand for energy and greater use of fossil fuels. As a result, the high emissions of
106 pollutants produce heavy pollutions in mega cities of eastern China, such as Beijing
107 and Shanghai. For example, in the city of Shanghai (a largest mega city in China), the
108 urban and economical developments of the city are very rapid. During 1990 to 2015,
109 the population increased from 13.3 to 24.1 million. The number of automobiles
110 increased from 0.2 million (1993) to 2.0 million (2011). The rapid growing population
111 and energy usage caused a rapid increase in the emissions of pollutants, leading to
112 severe air pollution problems in these mega cities (Zhang et al., 2006; Geng et al.,
113 2007; Deng et al., 2008).

114

115 Measurements, such as satellite observations have revealed much higher aerosol
116 pollution in eastern China than in eastern US (Tie et al., 2006). The high aerosol
117 pollution causes a wide range of environmental consequences. [Jia et al. \(2019\) studied](#)
118 [Anthropogenic Aerosol Pollution over the Eastern Slope of the Tibetan Plateau, and](#)
119 [Zhu et al \(2018\) studied the impact of smoke aerosols from Russian forest fires on the](#)
120 [air pollution over Asia](#). According to a study by Tie et al. (2009a), exposure to
121 extremely high particle concentrations leads to a great increase of lung cancer cases.
122 High PM (particular matter) concentrations also significantly reduce the range of
123 visibility in China's mega cities (Deng et al., 2008). According to a recent study, the
124 high aerosol pollution causes important effects on the crop (rice and wheat)
125 production in eastern China (Tie et al., 2016).

126

127 In the troposphere, ozone formation is resulted from a complicated chemical process,
128 and requires ozone precursors, such as VOCs (volatile organic carbons) and $\text{NO}_x =$
129 $\text{NO} + \text{NO}_2$ (nitrogen oxides) (Sillman, 1995). As the increase in industrial activity and
130 number of automobiles, the precursors of ozone (O_3) and the global budget of
131 oxidization are also significantly increased (Huang et al., 2017; Huang et al., 2018).
132 As a result, O_3 pollution becomes a serous pollution problem in Shanghai and other
133 Chinese mega cities (Geng et al., 2010; Tie 2009b; Tie et al., 2015). The effects on O_3
134 production rate can be characterized as either NO_x -sensitive or VOC-sensitive

Xuexi Tie 8/12/2019 7:51 PM
Formatted: Font:(Default) Times New
Roman, 12 pt

135 conditions. For the city areas, O₃ production is generally VOC-sensitive, while in the
136 remote area, O₃ production is generally NO_x-sensitive in eastern China (Sillman,
137 1995; Zhang et al., 2003; Lei et al., 2004; Tie et al., 2013). Thus, better understanding
138 the trends of O₃ precursors (VOCs, NO_x) is important to determine the O₃ trends in
139 Shanghai (as well as many large cities in China).

140 In the past few years, China's government made strong efforts to reduce the PM_{2.5}
141 pollutions. However, another important pollutant (O₃) becomes an important problem
142 in eastern China. Several studies regarding the O₃ formation are previously studied in
143 Shanghai. For example, Geng et al. (2007; 2008) study the relationship between O₃
144 precursors (NO_x and VOCs) for the ozone formation in Shanghai. Tie et al. (2009)
145 study the short-term variability of O₃ in Shanghai. Their study suggested that in
146 addition to the ozone precursors, meteorological conditions, such as regional transport,
147 have also strong impacts on the ozone concentrations. During September 2009, a
148 major field experiment (the MIRAGE-Shanghai) was conducted in Shanghai, and
149 multiply chemical species were measured during the experiment. The summary of the
150 measurements by Tie et al (2013) suggests that the ozone formation in Shanghai is
151 under VOC-sensitive condition. However, if the emission ration of NO_x/VOCs
152 reduces to a lower value (0.1-0.2), the ozone formation in Shanghai will switch from
153 VOC-sensitive condition to NO_x-sensitive condition.

154 Despite of some progresses have been made for the ozone formation in mega cities in
155 China, it is still lack of study of ozone development in large cities of China. For
156 example, this study shows that during late spring and early fall in eastern China,
157 under heavy PM_{2.5} pollutions, there were often strong O₃ chemical productions,
158 causing the co-occurrence of high PM_{2.5} and O₃ concentrations. Under heavy aerosol
159 condition, the solar radiation is depressed, significantly reducing the photochemical
160 production of O₃. This co-occurrence of high PM_{2.5} and O₃ is an unusual and is the
161 focus of this study. He and Carmichael (1999) suggest that aerosol particles can
162 enhance the scattering of solar radiation, enhancing the flux density inside the
163 boundary layer. Recent measurements also show that there were often high HONO
164 concentrations in major Chinese mega cities, especially during daytime, with
165 maximum concentrations ranging from 0.5 to 2 ppbv (Huang et al., 2017). Zhang et al.
166 (2016) suggest that there are several potential HONO sources, including surface

167 emissions, conversion of NO_2 at the ocean surface, etc., and adding these sources can
168 improve the calculated HONO concentrations. It is also interesting to note that the
169 high HONO surface concentrations were occurred during high aerosol concentration
170 periods, suggesting that there are additional HONO surface sources in eastern China.
171 Under the high daytime HONO concentrations, HONO can be photo-dissociated to be
172 OH radicals, which enhance the photochemical production of O_3 .

173

174 The paper is organized as follows: in Section 2, we describe the measurement of O_3
175 and $\text{PM}_{2.5}$. In Section 3, we describe the calculation of photo-dissociated rate of
176 HONO and a steady state model for the calculation of OH, and the causes of high O_3
177 production under the heavy aerosol condition. Section 4 shows a brief conclusion of
178 the results.

179

180 **2. Measurements of O_3 and $\text{PM}_{2.5}$**

181

182 There are long-term measurements in Eastern China by Chinese Environment
183 Protection Agency (CEPA) for monitoring the air quality in China. In eastern China,
184 especially in the capital city of China (Beijing), there are often heavy air pollutions,
185 especially for fine particular matter ($\text{PM}_{2.5}$ – the radius of particle being less than 2.5
186 μm). Figure 1 shows the measurement sites in Beijing, in which the measured
187 concentrations of $\text{PM}_{2.5}$ and O_3 are used to the analysis. In the region, the air
188 pollutions were very heavy, especially in winter (Long et al., 2016; Tie et al., 2017).
189 The previous studies suggested that the both aerosol and O_3 pollutions became the
190 major pollutants in the region (Li et al., 2017).

191

192 Figure 2 shows the daily averaged concentrations of $\text{PM}_{2.5}$ and O_3 in the Beijing
193 region in 2015. The daily averaged concentrations show that there were strong daily
194 and seasonal variations for both the concentrations of $\text{PM}_{2.5}$ and O_3 . Despite the daily
195 variation, the concentrations of $\text{PM}_{2.5}$ existed a strong seasonal variation. For example,
196 there were very high concentrations during winter, with maximum of $\sim 300 \mu\text{g}/\text{m}^3$.
197 While in summer, the maximum concentrations reduced to $\sim 150 \mu\text{g}/\text{m}^3$. The seasonal
198 variability of O_3 concentrations were opposite with the $\text{PM}_{2.5}$ concentrations, with
199 lower concentrations in winter ($< 50 \mu\text{g}/\text{m}^3$) and higher concentrations in summer ($>$

200 150 $\mu\text{g}/\text{m}^3$). These seasonal variations of $\text{PM}_{2.5}$ and O_3 have been studied by previous
201 studies (Tie and Cao, 2017; Li et al., 2017). Their results suggest that the winter high
202 $\text{PM}_{2.5}$ concentrations were resulted from the combination of both the high emissions
203 (heating season in the Beijing region), and poor meteorological ventilation conditions,
204 such as lower PBL (Planetary Boundary Layer) height (Quan et al., 2013; Tie et al.
205 2015). According to the photochemical theory of O_3 formation, the summer high and
206 winter low O_3 concentrations are mainly due to seasonal variation of the solar
207 radiation (Seinfeld, J. H. and Pandis, 2006).

208

209 The heavy aerosol concentrations play important roles to reduce solar radiation,
210 causing the reduction of O_3 formation. (Bian et al., 2007). As we show in Fig. 3
211 (upper panel), during wintertime, the O_3 concentrations were strong anti-correlated
212 with the $\text{PM}_{2.5}$ concentrations, suggesting that the reduction of solar radiation by
213 aerosol particles have important impact on the reduction of O_3 concentrations. Figure
214 3 (upper panel) also shows that the relationship between O_3 and $\text{PM}_{2.5}$ was not
215 linearly related. For example, when the concentrations of $\text{PM}_{2.5}$ were less than 100
216 $\mu\text{g}/\text{m}^3$, O_3 concentrations rapidly decreased with the increase of $\text{PM}_{2.5}$ concentrations.
217 In contrast, when the concentrations of $\text{PM}_{2.5}$ were greater than 100 $\mu\text{g}/\text{m}^3$, O_3
218 concentrations slowly decreased with the increase of $\text{PM}_{2.5}$ concentrations. This is
219 consistent with the result of Bian et al (2007).

220

221 It is interesting to note that from late spring to early fall periods, the correlation
222 between $\text{PM}_{2.5}$ and O_3 concentrations was positive relationship compared to the
223 negative relationship in winter (see Fig. 3 (lower panel)). This result suggests that O_3
224 production was high during the heavy haze period, despite the solar radiation was
225 greatly depressed. In order to clearly display this unusual event, we illustrate diurnal
226 variations of $\text{PM}_{2.5}$ and O_3 , and NO_2 during a fall period (from Oct.5 to Oc. 6, 2015).
227 Figure 4 shows that during this period (as a case study), the $\text{PM}_{2.5}$ concentrations were
228 very high, ranging from 150 to 320 $\mu\text{g}/\text{m}^3$. Under such high aerosol condition, the
229 solar radiation should be significantly reduced, and O_3 photochemical production
230 would be reduced. However, the diurnal variation of O_3 was unexpectedly strong,
231 with high noontime concentration of $>220 \mu\text{g}/\text{m}^3$ and very low nighttime
232 concentration of $\sim 25 \mu\text{g}/\text{m}^3$. This strong diurnal variation was due to the
233 photochemical activity, which suggested that during relatively low solar conditions,

234 the photochemical activities of O₃ production was high. According to the theory of
235 the O₃ chemical production, the high O₃ production is related to high oxidant of OH
236 (Seinfeld and Pandis, 2006), which should not be occurred during lower solar
237 radiation. This result brings important issue for air pollution control strategy, because
238 both PM_{2.5} and O₃ are severe air pollutants in eastern China.

239

240 To clearly understand the effect of the high aerosol concentrations on solar radiation,
241 we investigate the meteorological conditions, such as cloud covers, relation humidity
242 (RH), and solar radiation during the period of the case study (see Figs. 5 and 6).
243 Figure 5 shows that the cloud condition was close to the cloud free condition, but
244 there was a very heavy aerosol layer in the Beijing region, suggesting that cloud cover
245 played a minor role in the reduction of the solar radiation. The measured RH values
246 (not shown) were generally higher than 60%, with a maximum of 95% during the
247 period. As a result, the high aerosol concentrations companied by high RH produced
248 important effects on solar radiation. As shown in Fig. 6, the daytime averaged solar
249 radiation was significantly reduced (about 40% reduction in Oct. 5-6 period compared
250 with the value of Oct. 8).

251

252 **3. Method**

253

254 In order to better understand the O₃ chemical production occurred in heavy aerosol
255 condition in eastern China, the possible O₃ production in such condition is discussed.
256 Ozone photochemical production (P[O₃]) is strongly related to the amount of OH
257 radicals (Chameides et al., 1999). According to the traditional theory, the amount of
258 surface OH radicals is proportional to the surface solar radiation, which is represented
259 by

260

$$261 \quad [\text{OH}] = \text{P}[\text{HOx}]/\text{L}[\text{HOx}]^* \quad (\text{R-1})$$

262

263 Where [OH] represents the concentration of hydroxyl radicals (#/cm³); HOx
264 represents the concentration of HO₂ + OH (#/cm³); P[HOx] represents the
265 photochemical production of HOx (#/cm³/s); and L[HOx]* (1/s) represents the
266 photochemical destruction of HOx, which is normalized by the concentrations of OH.

267

268 The major process for the photochemical production of P[HOx] is through the O₃
269 photolysis and follows by the reaction with atmospheric water vapor. It can be
270 expressed as

$$271 \quad P[\text{HOx}] = J_1[\text{O}_3]/(k_1 \times \text{am}) \times 2.0 \times k_2[\text{H}_2\text{O}] = P_1[\text{HOx}] \quad (\text{R-2})$$

272

273 Where J₁ represents the photolysis of O₃ + hν → O¹D; k₁ represents the reaction rate
274 of O¹D + am → O³P; and k₂ represents the reaction rate of O¹D + H₂O → 2OH. As
275 we can see, this HOx production is proportional to the magnitude of solar radiation
276 (J₁), and J₁ is the O₃ photolysis with the solar radiation. Figure 7 shows the
277 relationship between the values of J₁ and aerosol concentrations in October at
278 middle-latitude calculated by the TUV model (Madronich and Flocke, 1999). This
279 result suggests that under the high aerosol concentrations (AOD = 2.5), the J₁ value is
280 strongly depressed, resulting in significant reduction of OH concentrations and O₃
281 production. For example, the maximum J₁ value is about 2.7×10⁻⁵ (1/s) with lower
282 aerosol values (AOD = 0.25). According to the previous study, the surface PM_{2.5}
283 concentrations were generally smaller than 50 μg/m³ with this AOD value (Tie et al.,
284 2017). However, when the AOD value increase to 2.5 (the PM_{2.5} concentrations are
285 generally >100 μg/m³), the maximum J₁ value rapidly decreases to about 6×10⁻⁶ (1/s),
286 which is about 450% reduction compared to the value with AOD=0.25. This study
287 suggests that under high PM_{2.5} concentrations (>100 μg/m³), the photochemical
288 production of OH (P[HOx]) is rapidly decreased, leading to low OH concentrations,
289 which cannot initiate the high oxidation of O₃ production. As a result, the high O₃
290 production shown in Fig. 4 cannot be explained. Other sources for O₃ oxidation are
291 needed to explain this result.

292

293 Recent studies show that the HONO concentrations are high in eastern China (Huang
294 et al., 2017). Because under high solar radiation, the photolysis rate of HONO is very
295 high, resulting in very low HONO concentrations in daytime (Seinfeld and Pandis,
296 2006). These measured high HONO concentrations are explained by their studies.
297 One of the explanations is that there are high surface HONO sources during daytime,
298 which produces high HONO concentrations (Huang et al., 2017). Zhang et al. (2016)
299 suggest that there are several potential HONO sources, including surface emissions,
300 conversion of NO₂ at the ocean surface, etc. Zhang et al. (2016) parameterized these

301 potential HONO sources in the WRF-Chem model, and the calculated HONO
302 concentrations are increased in the WRF-Chem model.

303

304 The version of the WRF-Chem model is based on the version developed by Grell et al.
305 (2015), and is improved mainly by Tie et al. (2017) and Li et al. (2011). The chemical
306 mechanism chosen in this version of WRF-Chem is the RADM2 (Regional Acid
307 Deposition Model, version 2) gas-phase chemical mechanism. For the calculation of
308 HONO, only the gas-phase chemistry of OH+NO is included to calculate HONO
309 concentrations. As shown in Fig. 8, the calculated HONO concentrations are
310 significantly smaller than the measured HONO values in eastern China, suggesting
311 that in addition to the gas-reaction, there are missing HONO sources (surface sources
312 or others). Because these missing sources are not fully understood and large
313 uncertainty is remained, in the following calculation, we compare the OH
314 concentrations due to both calculated HONO (without the missing sources) and the
315 measured HONO concentrations to illustrate the importance of these missing sources
316 for the production of OH radicals and to suggest that further study to better
317 understand the missing sources is an urgent scientific issue.

318

319 Figure 8 shows the measured HONO concentrations in three large cities in China
320 (Shanghai, Xi'an, and Beijing) during fall and winter. It also shows the corresponding
321 PM_{2.5} and O₃ in the 3 cities (i.e., Fig. 8a for Beijing, Fig. 8b for Shanghai, and Fig. 8c
322 for Xian). It shows that the measured HONO concentrations were high, ranging from
323 sub-ppbv to a few ppbv, with higher values during morning, and lower values in
324 daytime. The co-occurrences of high PM_{2.5} and O₃ happened in the 3 cities. As a
325 result, we think that the high HONO is a common event in large cities in eastern
326 China, especially in daytime. This high HONO is also measured by previous studies
327 (Zhang et al. 2016; Huang et al. 2017). In this study, we make an assumption that the
328 co-occurrence between O₃ and PM_{2.5} occurred under high HONO concentrations. We
329 note that using this assumption may result in some uncertainties in estimating the
330 effect of HONO on OH. For example, using the measured HONO in Xi'an and
331 Beijing could produce 1-2 times higher OH production by photolysis of HONO than
332 the result by using the data from Shanghai. In this case, we use the measured HONO
333 from Shanghai to avoid the over estimate of the HONO effect, which can be
334 considered as a low-limit estimation.

335

336 It is also interesting to note that the high HONO concentrations were occurred during
337 high aerosol concentration periods. Figure 9 illustrates that when the PM_{2.5}
338 concentrations increased to 70-80 $\mu\text{g}/\text{m}^3$, and the HONO concentrations enhanced to
339 1.4-18 ppbv during September in Shanghai. This measured high HONO
340 concentrations were significantly higher than the calculated concentrations (shown in
341 Fig. 8), suggesting that some additional sources of HONO are needed. This result is
342 consistent with the HONO measurements in other Chinese cities (Huang et al. 2017).

343

344 The high HONO concentrations in daytime become a significant source of OH
345 radicals. As a result, the OH production rate (P[HOx]) can be written to the following
346 reactions.

347

$$348 \quad P_2[\text{HOx}] = J_2 \times [\text{HONO}] \quad (\text{R-3})$$

$$349 \quad P[\text{HOx}] = P_1[\text{HOx}] + P_2[\text{HOx}]$$

$$350 \quad = J_1[\text{O}_3]/(k_1 \times \text{am}) \times 2.0 \times k_2[\text{H}_2\text{O}] + J_2 \times [\text{HONO}] \quad (\text{R-4})$$

351

352 Because the chemical lifetime of OH is less than second, OH concentrations can be
353 calculated according to equilibrium of chemical production and chemical loss. With
354 the both OH chemical production processes, the OH concentrations can be calculated
355 by the following equation (Seinfeld and Pandis, 2006).

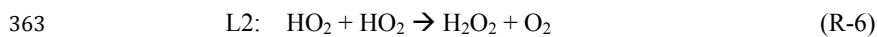
356

$$357 \quad P_1 + P_2 = L_1 + L_2$$

358

359 Where P1 and P2 are the major chemical productions, expressed in R-4, and L1 and
360 L2 are the major chemical loss of OH, and represent by

361



364

365 Under high NOx condition, such as in the large cities in eastern China, NOx
366 concentrations were often higher to 50 ppbv (as shown in Fig. 4). As a result, the L1
367 term is larger than L2. The OH concentrations can be approximately expressed as

368

369
$$[\text{HO}] = \frac{\{J_1[\text{O}_3]/(k_1 \times \text{am}) \times 2.0 \times k_2[\text{H}_2\text{O}] + J_2 \times [\text{HONO}]\}}{k_3[\text{NO}_2]}$$

370 (R-5)
371

372 Where k_3 is the reaction coefficient of $\text{OH} + \text{NO}_2 \rightarrow \text{HNO}_3$.

373

374 **4. Result and analysis**

375

376 **4.1. OH productions in different HONO conditions**

377

378 In order to quantify the individual effects of these two OH production terms (P1 and
379 P2) on the OH concentrations, the P1 and P2 are calculated under different daytime
380 HONO conditions (calculated low HONO and measured high HONO concentrations).

381 Figure 10 shows that under the low HONO condition, the P1 is significantly higher
382 than P2, and P2 has only minor contribution to the OH values. For example, the
383 maximum of P1 occurred at 13 pm, with a value of $65 \times 10^6 \text{ \#/cm}^3/\text{s}$. In contrast, the
384 maximum of P2 occurred at 10 am, with a value of $15 \times 10^6 \text{ \#/cm}^3/\text{s}$. However, under
385 high HONO condition, the P2 plays very important roles for the OH production. The
386 maximum of P2 occurred at 11 am, with a value of $350 \times 10^6 \text{ \#/cm}^3/\text{s}$, which is about
387 500% higher than the P1 value. It is important to note that this calculation is based on
388 the high aerosol condition (AOD = 2.5) in September. This result can explain the high
389 O_3 chemical production in Fig. 4.

390

391 **4.2. OH in different aerosol conditions**

392

393 In order to understand the effect of aerosol conditions, especially high aerosol
394 conditions, on the OH concentrations. Figure 11 shows the OH concentrations with
395 and without HONO production of OH. With including the HONO production (i.e.,
396 including P1 and P2), the calculated OH concentrations are significantly higher than
397 without including this production (i.e., only including P1). The both calculated OH
398 concentrations are rapidly changed with different levels of aerosol conditions. For
399 example, without HONO production, the maximum OH concentration is about
400 $7.5 \times 10^5 \text{ \#/cm}^3$ under low aerosol condition (AOD=0.25). In contrast, the maximum
401 OH concentration rapidly reduced to $1.5 \times 10^5 \text{ \#/cm}^3$ under high aerosol condition
402 (AOD=2.5), and further decreased to $1.0 \times 10^5 \text{ \#/cm}^3$ with the AOD value of 3.5. In
403 contrast, with including HONO production, the OH concentrations significantly

404 increased. Under higher aerosol condition (AOD=2.5), the maximum of OH
405 concentration is about $7.5 \times 10^5 \text{ \#/cm}^3$, which is the same value under low aerosol
406 condition in the no-HONO case. This result suggests that the measured high O₃
407 production occurred in the high aerosol condition is likely due to the high HONO
408 concentrations in Shanghai.

409

410 **4.3. Effects of clouds**

411

412 Cloud cover can have very important impacts on the photolysis of HONO, which can
413 affect the effect of HONO on the OH radicals. The above calculations are based on
414 the cloud-free condition, with heavy aerosol concentration in the Beijing region. As
415 shown in Fig. 5, during the case study period (Oct 5 to 6, 2015) (see Fig. 4), the
416 weather map shows that the cloud-free condition, with heavy aerosol condition.

417

418 In order to understand the effects of cloud on the photolysis of HONO, we include
419 different cloud covers in the TUV model. The calculated results show in Fig. 12.
420 The results show that the thin cloud (with cloud cover in 2 km and cloud water of 10
421 g/m^3), could reduce the photolysis rate of HONO by about 40%, but the HONO could
422 still remain important effects. However, with dense cloud condition (with cloud
423 covers at 2 and 3 km and cloud water of 50 g/m^3), the photolysis rate of HONO
424 could reduce by 9-10 times by the cloud. In this case, adding photolysis rate of
425 HONO cannot produce important effect on OH radicals and the production of O₃.

426

427 **4.4. OH in winter**

428

429 The measurement of O₃ also shows that the concentrations in winter were always low
430 (see Fig. 2), suggesting that the O₃ concentrations were not significantly affected by
431 the appearance of HONO. Figure 13 shows the OH concentrations in September and
432 December. It shows that under different aerosol conditions, OH concentrations in
433 December were very low compared with the values in September. Both the calculated
434 OH concentrations include the HONO production term. For example, under the
435 condition of AOD=2.5, the maximum OH is about $7.5 \times 10^5 \text{ \#/cm}^3$ in September, while
436 it rapidly reduces to $1.5 \times 10^5 \text{ \#/cm}^3$ in December. Under the condition of AOD=3.5,
437 the maximum OH is still maintaining to a relative high level ($4.5 \times 10^5 \text{ \#/cm}^3$) in
438 September. However, the maximum OH values are extremely low in December, with

439 maximum value of $0.5 \times 10^5 \text{ \#/cm}^3$ in December. Because both the OH chemical
440 productions (P1 and P2) are strongly dependent upon solar radiation (see equation
441 R-4), the seasonal variation of solar radiation plays important roles for controlling the
442 OH production in winter (see Fig. 13). Because the solar radiation is in a very low
443 level in winter, adding the photolysis of HONO has smaller effect in winter than in
444 other seasons and OH remains low values by including the HONO production term.

445

446 **Summary**

447

448 Currently, China is undergoing a rapid economic development, resulting in a high
449 demand for energy, greater use of fossil fuels. As a result, the high emissions of
450 pollutants produce heavy aerosol pollutions ($\text{PM}_{2.5}$) in eastern China, such as in the
451 mega city of Beijing. The long-term measurements show that in addition to the heavy
452 aerosol pollution, the O_3 pollution becomes another major pollutants in the Beijing
453 region. The measured results show that there were very strong seasonal variation in
454 the concentrations of both $\text{PM}_{2.5}$ and O_3 in the region. During winter, the seasonal
455 variability of O_3 concentrations were anti-correlated with the $\text{PM}_{2.5}$ concentrations.
456 However, from late spring to early fall, the correlation between $\text{PM}_{2.5}$ and O_3
457 concentrations was positive compared to the negative in winter. This result suggests
458 that during heavy aerosol condition (the solar radiation was depressed), the O_3
459 chemical production was still high, appearing a co-occurrence of high $\text{PM}_{2.5}$ and O_3 in
460 some cases from late spring to early fall. This co-occurrence of high $\text{PM}_{2.5}$ and O_3 is
461 the focus of this study. The results are highlighted as follows;

462

463 (1) There are high daytime HONO concentrations in major Chinese mega cities, such
464 as in Beijing and Shanghai. It is also interesting to note that the high HONO
465 concentrations were occurred during high aerosol concentration periods. Under
466 the high daytime HONO concentrations, HONO can be photo-dissociated to be
467 OH radicals, and becomes an important process to produce OH.

468 (2) With including the OH production of measured HONO concentrations, the
469 calculated OH concentrations are significantly higher than without including this
470 production. For example, without HONO production, the maximum OH
471 concentration is about $7.5 \times 10^5 \text{ \#/cm}^3$ under low aerosol condition ($\text{AOD}=0.25$),
472 and rapidly reduced to $1.5 \times 10^5 \text{ \#/cm}^3$ under high aerosol condition ($\text{AOD}=2.5$) in

473 September. In contrast, by including HONO production, the OH concentrations
474 significantly increased. For example, under higher aerosol condition (AOD=2.5),
475 the maximum of OH concentration is about $7.5 \times 10^5 \text{ #/cm}^3$, which is similar to the
476 value under low aerosol condition in the no-HONO case. This result suggests that
477 even under the high aerosol conditions, the chemical oxidizing process for O₃
478 production can be active. This result is likely for explaining the co-occurrence of
479 high PM_{2.5} and high O₃ from late spring to early in eastern China.

480 (3) The measurement of O₃ also shows that the concentrations in winter were always
481 low, suggesting that the O₃ concentrations were not significantly affected by the
482 appearance of HONO. The calculated result shows that the seasonal variation of
483 solar radiation plays important roles for controlling the OH production in winter.
484 Because the solar radiation is in a very low level in winter, adding the photolysis
485 of HONO has smaller effect in winter than in other seasons, and OH remains low
486 values by including the HONO production term.

487 In recent years, the PM_{2.5} pollutions are reduced due to the large control efforts by the
488 Chinese government, the O₃ pollutions become another severe pollution problem in
489 eastern China. This study is important, because it provides some important scientific
490 highlights to better understand the O₃ pollutions in eastern China.

491

492 **Data availability.** The data used in this paper can be provided upon request from
493 Xuexi Tie (tiexx@ieecas.cn).

494

495 **Author contributions.** XT came up with the original idea of investigating the
496 scientific issue. XT and JX designed the analysis method. XL, GL and SZ provided
497 the observational data and helped in discussion. XT prepared the manuscript with
498 contributions from all co-authors.

499

500 **Acknowledgement**

501 This work was supported by the National Natural Science Foundation of China
502 (NSFC) under Grant Nos. 41430424 and 41730108. The Authors thanks the supports
503 of Center for Excellence in Urban Atmospheric Environment, Institute of Urban
504 Environment, Chinese Academy of Sciences.

505

506

507 **References**

508

509 Bian H., S.Q. Han, X. Tie, M.L. Shun, and A.X. Liu, Evidence of Impact of Aerosols
510 on Surface Ozone Concentration: A Case Study in Tianjin, China, *Atmos.*
511 *Environ.*, *41*, 4672-4681, 2007.

512 Chameides, W. L., Fehsenfeld, F., Rodgers, M. O., Cardelino, C., Martines, J., Parrish,
513 D., Lonneman, W., Lawson, D. R., Ras-
514 mussen, R. A., Zimmerman, P.,
515 Greenberg, J., Middleton, P., and Wang, T.: Ozone precursor relationships in the
ambient atmo- sphere, *J. Geophys. Res.*, *97*, 6037–6055, 1992.

516 Deng X.J, X Tie, D. Wu, XJ Zhou, HB Tan, F. Li, C. Jiang, Long-term trend of
517 visibility and its characterizations in the Pearl River Delta Region (PRD), China,
518 *Atmos. Environ.*, *42*, 1424-1435, 2008.

519

520 Geng, F.H., C.S., Zhao, X. Tang, GL. Lu, and X. Tie, Analysis of ozone and VOCs
521 measured in Shanghai: A case study, *Atmos. Environ.*, *41*, 989-1001, 2007.

522 Geng, FH, CG Cai, X. Tie, Q. Yu, JL An, L. Peng, GQ Zhou, JM Xu, Analysis of
523 VOC emissions using PCA/APCS receptor model at city of Shanghai, China, *J.*
524 *Atmos. Chem.*, *62*, 229–247, DOI :10.1007/s10874-010-9150-5, 2010.

525

526 Grell, G. A., Peckham, S. E., Schmitz, R., McKeen, S. A., Frost, G., Skamarock, W.
527 C., and Eder, B.: Fully coupled “online” chemistry within the WRF model, *Atmos.*
528 *Environ.*, *39*, 6957– 6975,2005.

529

530 He, S., & Carmichael, G. R. (1999). Sensitivity of photolysis rates and ozone pro-
531 duction in the troposphere to aerosol properties. *Journal of Geophysical*
532 *Research: Atmospheres*, 104(D21), 26307-26324.

533

534 Huang, J.P, X. Y. Liu, C. Y. Li, L. Ding, H. P. Yu, The global oxygen budget and its
535 future projection. *Science Bull.* *63*, 1180–1186, 2018.

536

537 Huang J., Y. Li, C. Fu, F. Chen, Q. Fu, A. Dai, M. Shinoda, Z. Ma, W. Guo, Z. Li, L.
538 Zhang, Y. Liu, H. Yu, Y. He, Y. Xie, X. Guan , M. Ji, L. Lin, S. Wang, H. Yan
539 and G. Wang, Dryland climate change recent progress and challenges. *Rev. of*
540 *Geophys.*, *55*, 719-778, doi:10.1002/2016RG000550, 2017.

541 Huang, R. J., L. Yang, JJ Cao, QY Wang, X. Tie, et al., Concentration and sources of
542 atmospheric nitrous acid (HONO) at an urban site in Western China. *Sci. of Total*
543 *Environ.*, 593-594, 165-172, doi.org/10.1016/j.scitotenv.2017.02.166, 2017.

544 Jia R., M. Luo, Y. Liu, Q. Z. Zhu, S. Hua, C. Q. Wu and T. B. Shao, 2019:
545 Anthropogenic Aerosol Pollution over the Eastern Slope of the Tibetan Plateau.
546 *Advances in Atmospheric Sciences*, 36(8): 847-862, 2019.

547 Lei, W., R. Zhang, X. Tie, P. Hess, Chemical characterization of ozone formation in
548 the Houston-Galveston area, *J. Geophys. Res.*, *109*, doi:10.102/2003JD004219,
549 2004.

Xuexi Tie 8/12/2019 7:55 PM

Formatted: Font:(Default) Times New Roman, 12 pt

Xuexi Tie 8/12/2019 7:55 PM

Formatted: Font:(Default) Times New Roman, 12 pt, Italic

Xuexi Tie 8/12/2019 7:55 PM

Formatted: Font:(Default) Times New Roman, 12 pt

- 550 Li, G., Bei, N., Tie, X., and Molina, L. T.: Aerosol effects on the photochemistry in
551 Mexico City during MCMA-2006/MILAGRO campaign, *Atmospheric Chemistry*
552 *and Physics*, 11, 5169–5182, 2011.
- 553
- 554 Li, G., Bei, N., Cao, J., Wu, J., Long, X., Feng, T., Dai, W., Liu, S., Zhang, Q., and
555 Tie, X.: Widespread and persistent ozone pollution in eastern China during the
556 non-winter season of 2015: observations and source attributions, *Atmos. Chem.*
557 *Phys.*, 17, 2759-2774, doi:10.5194/acp-17-2759-2017, 2017.
- 558 Long, X., X. Tie, JJ Cao, RJ Huang, T. Feng, N. Li, SY Zhao, J. Tian, GH Li, Q.
559 Zhang, Impact of crop field burning and mountains on heavy haze in the North
560 China Plain: A case study, *Atmos. Chem. Phys.*, 16, 9675-9691,
561 doi:10.5194/acp-16-9675-2016, 2016.
- 562 Madronich, S. & Flocke, S. in *Environmental Photochemistry 2 / 2L*, 1–26 (Springer
563 Berlin Heidelberg, 1999)
- 564 Quan, J.N., Y. Gao, Q. Zhang, X. Tie*, JJ Cao, SQ Han, JW Meng, PF Chen, DL
565 Zhao, Evolution of Planetary Boundary Layer under different weather conditions,
566 and its impact on aerosol concentrations, *Particuology*, doi:
567 10.1016/j.partic.2012.04.005, 2013.
- 568 Seinfeld, J. H. and Pandis, S. N.: *Atmospheric Chemistry and Physics: From Air*
569 *Pollution to Climate Change*, 2nd Edn., John Wiley and Sons, New York, 2006.
- 570 Shi, C., Wang, S., Liu, R., Zhou, R., Li, D., Wang, W., ... & Zhou, B. (2015). A study
571 of aerosol optical properties during ozone pollution episodes in 2013 over
572 Shanghai, China. *Atmospheric Research*, 153, 235-249.
- 573 Sillman, S.: The use of NO_y, H₂O₂, and HNO₃ as indicators for
574 ozone-NO_x-hydrocarbon sensitivity in urban locations, *J. Geo- phys. Res.*, 100,
575 14175–14188, 1995.
- 576 Tie, X., G. Brasseur, C. Zhao, C. Granier, S. Massie, Y. Qin, P.C. Wang, GL Wang,
577 PC, Yang100., Chemical Characterization of Air Pollution in Eastern China and
578 the Eastern United States, *Atmos. Environ.*, 40. 2607-2625, 2006.
- 579
- 580 Tie, X., Madronich, S., Li, G., Ying, Z., Zhang, R., Garcia, A., Taylor, J., and Liu, Y.:
581 Characterizations of chemical oxidants in Mexico City: A regional chemical
582 dynamical model (WRF-Chem) study, *Atmospheric Environment*, 41, 1989-2008,
583 2007.
- 584 Tie, X., D. Wu, and G. Brasseur, Lung Cancer Mortality and Exposure to
585 Atmospheric Aerosol Particles in Guangzhou, China, *Atmos. Environ*, 43, 2375–
586 2377, 2009a.
- 587 Tie, X., FH. Geng. L. Peng, W. Gao, and CS. Zhao, Measurement and modeling of O₃
588 variability in Shanghai, China; Application of the WRF-Chem model, *Atmos.*

589 *Environ.*, 43, 4289-4302, 2009b.

590 Tie X., F. Geng, A. Guenther, J. Cao, J. Greenberg, R. Zhang, E. Apel, G. Li,
 591 A. Weinheimer, J. Chen, and C. Cai, Megacity impacts on regional ozone
 592 formation: observations and WRF-Chem modeling for the MIRAGE-Shanghai
 593 field campaign, *Atmos. Chem. Phys.*, 13, 5655-5669, doi:10.5194/acp-13-5655-2013, 2013.

595 Tie, X., Q. Zhang, H. He, JJ Cao, SQ Han, Y. Gao, X. Li, and XC Jia, A budget
 596 analysis on the formation of haze in Beijing, *Atmos. Environ.*, 25-36, 2015.

597 Tie, X., RJ Huang, WT Dai, JJ Cao, X. Long, XL Su, SY Zhao, QY Wang, GH Li,
 598 Effect of heavy haze and aerosol pollution on rice and wheat productions in China,
 599 *Sci. Rep.* 6, 29612; doi: 10.1038/srep29612, 2016.

600 Tie, X., J.J. Cao, Understanding Variability of Haze in Eastern China, *J Fundam*
 601 *Renewable Energy Appl*, 7:6 DOI: 10.4172/2090-4541.100024, 2017.

602 Tie, X., R.J. Huang, J.J. Cao, Q. Zhang, Y.F. Cheng, H. Su, D. Chang, U. Pöschl, T.
 603 Hoffmann, U. Dusek, G. H. Li, D. R. Worsnop, C. D. O'Dowd, Severe Pollution
 604 in China Amplified by Atmospheric Moisture, *Sci. Rep.* 7: 15760 |
 605 DOI:10.1038/s41598-017-15909-1, 2017.

606 Zhang, L., Wang, T., Zhang, Q., Zheng, J., Xu, Z., & Lv, M.. Potential sources of
 607 nitrous acid (HONO) and their impacts on ozone: A WRF/Chem study in a
 608 polluted subtropical region. *Journal of Geophysical Research: Atmospheres*,
 609 121(7), 3645- 3662, 2016.

610 Zhang, R., X. Tie, and D. Bond, Impacts of Anthropogenic and Natural NO_x Sources
 611 over the U.S. on Tropospheric Chemistry, *Proceedings of National Academic*
 612 *Science USA*, 100, 1505-1509, 2003.

614 Zhang, Q., C. Zhao, X. Tie, Q. Wei ,G. Li, and C. Li, Characterizations of Aerosols
 615 over the Beijing Region: A Case Study of Aircraft Measurements, 40,
 616 4513-4527, *Atmos. Environ.*, 2006.

617 [Zhu Q., Y. Liu, R. Jia, S. Hua, T. Shao, B. Wang: A numerical simulation study on the impact of](#)
 618 [smoke aerosols from Russian forest fires on the air pollution over Asia. *Atmos. Environ.*](#)
 619 [182,263-274, 2018](#)

620
621

Xuexi Tie 8/12/2019 7:57 PM
 Formatted: Font:(Default) Times New Roman, 12 pt, Italic

Xuexi Tie 8/12/2019 7:57 PM
 Formatted: Font:(Default) +Theme Body, 10.5 pt

622 **Figure Caption**

623

624 **Fig. 1.** The geographic locations of the measurement sites in Beijing, in which the
625 measured concentrations of PM_{2.5} and O₃ are used to the analysis.

626

627 **Fig. 2.** The daily averaged concentrations of PM_{2.5} and O₃ in the Beijing region in
628 2015. The concentrations are averaged over all sites shown in Fig. 1. The blue lines
629 represent the PM_{2.5} concentrations (μg/m³), and the red bars represent the O₃
630 concentrations (μg/m³). The rectangles show some typical events during winter
631 (green), spring and fall (orange), and summer (red).

632

633 **Fig. 3.** The correlation between O₃ and PM_{2.5} concentrations during winter (upper
634 panel) and from late spring to early fall (lower panel). During winter, O₃
635 concentrations were strong anti-correlated with the PM_{2.5} concentrations. From late
636 spring to early fall, O₃ concentrations were correlated with the PM_{2.5} concentrations.

637

638 **Fig. 4.** The diurnal variations of PM_{2.5} (blue line) and O₃ (red line), and NO₂ (green
639 line) during a fall period (from Oct.5 to Oct. 6, 2015). It shows that with high PM_{2.5}
640 condition, there was a strong O₃ diurnal variation.

641

642 **Fig. 5.** The cloud condition during the period of the case study (between Oct 5 and 6,
643 2015) in the Beijing region. The bright white color shows the cloud covers, and the
644 grey white shows the haze covers. The Beijing region was under the heavy haze
645 conditions during the period.

646

647 **Fig. 6.** The measured solar radiation (W/m²) from Oct. 3 to Oct. 9, 2015 in Beijing.
648 The upper panel shows hourly values, and the lower panel shows the daytime
649 averaged values.

650

651 **Fig. 7.** The effect of aerosol levels with AOD = 0.25 (black line), AOD = 2.5 (red
652 line), AOD = 3.5 (blue line), and AOD = 4.0 (green line) on the O₃ photolysis
653 calculated by the TUV model in October at middle-latitude.

654

655 **Fig. 8a.** The measured HONO concentrations (ppbv) and the PM_{2.5} and O₃ daily
656 concentrations in Beijing. The upper panel shows the measured daily concentrations
657 of PM_{2.5} and O₃ as shown in Fig.2. The dark-red line was measured HONO in Beijing
658 from 1 to 27 January, 2014.

659

660 **Fig. 8b.** The measured HONO concentrations (ppbv) and the PM_{2.5} and O₃ daily
661 concentrations in Shanghai. The upper panel shows the measured daily concentrations
662 of PM_{2.5} and O₃ in 2015. The dark-red line was measured in Shanghai from 9 to 18
663 September, 2009. The green line was calculated by the WRF-Chem model.

664

665 **Fig. 8c.** The measured HONO concentrations (ppbv) and the PM_{2.5} and O₃ daily
666 concentrations in Xi'an. The upper panel shows the measured daily concentrations of
667 PM_{2.5} and O₃ in 2015. The red line was measured HONO in Xi'an from 24 July to
668 August 6, 2015.

669

670 **Fig. 9.** The measured HONO (upper left panel), PM_{2.5} concentrations (lower left
671 panel), and O₃ concentrations (upper right panel) in fall in Shanghai. It illustrates that

672 the high HONO concentrations were corresponded with high PM_{2.5} concentrations.

673

674 **Fig. 10.** The calculated OH production P(HOx) (#/cm³/s) by using the model
675 calculated HONO (low concentrations) (in the upper panel) and by using the
676 measured HONO (high concentrations) (in the lower panel). The red bars represent
677 the calculation of the P1 term, and the red bars represent the calculation of the P2
678 term (OH production from HONO).

679

680 **Fig. 11.** The calculated OH concentrations (#/cm³) with (upper panel) and without
681 (lower panel) HONO production of OH, under different aerosol levels. Dark red
682 (AOD=0.25), red (AOD=2.5), red (AOD=3.5), and red (AOD=4.0).

683

684 **Fig. 12.** The effect of cloud cover on the photolysis rate of HONO (J[HONO]). The
685 blue, red, and green lines represent the cloud water vapor of 0 (cloud-free), 10 (g/m³ –
686 thin cloud), and 50 (g/m³ – thick cloud), respectively. The left panel (A) represents
687 the light aerosol condition, with AOD of 0.25, and the right panel (B) represents the
688 heavy aerosol condition, with AOD of 2.5.

689

690 **Fig. 13.** The calculated OH concentrations in September (blue bars) and December
691 (dark red bars), under different aerosol levels.

692

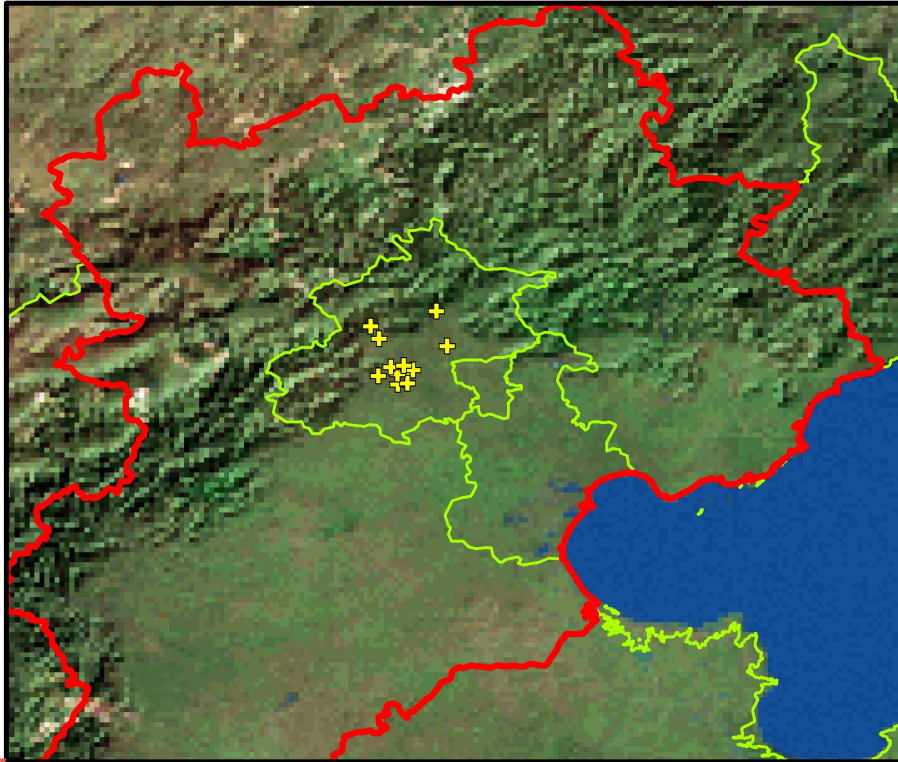
693

694

695

696
697

Figures

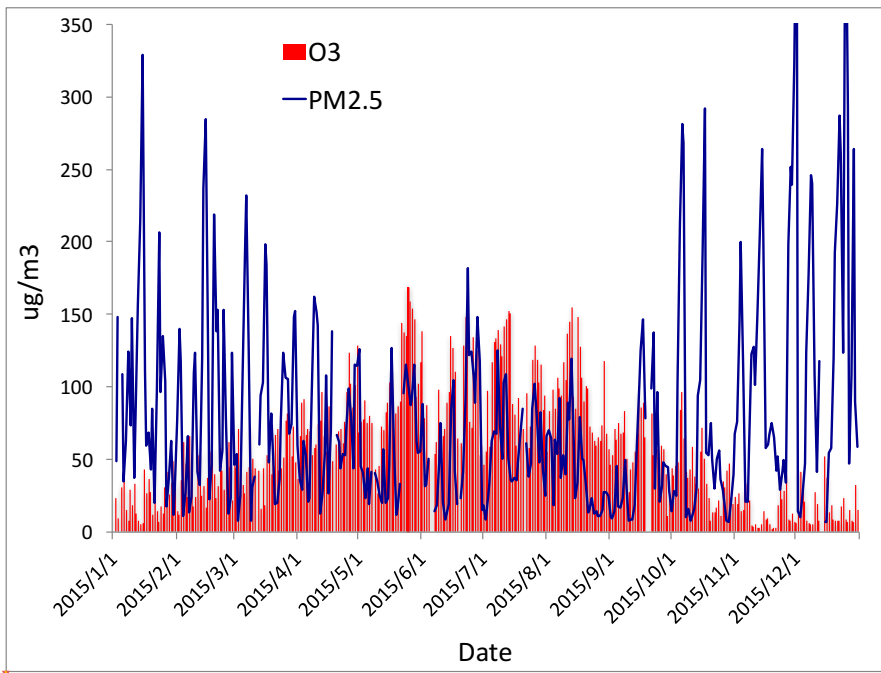


698
699
700
701
702

Fig. 1. The geographic locations of the measurement sites in Beijing, in which the measured concentrations of $PM_{2.5}$ and O_3 are used to the analysis.

Xuexi Tie 8/13/2019 11:59 AM

Deleted: <sp>



704
705
706
707
708
709
710
711
712
713
714
715

Fig. 2. The daily averaged concentrations of PM_{2.5} and O₃ in the Beijing region in 2015. The concentrations are averaged over all sites shown in Fig. 1. The blue lines represent the PM_{2.5} concentrations (μg/m³), and the red bars represent the O₃ concentrations (μg/m³). The rectangles show some typical events during winter (green), spring and fall (orange), and summer (red).

Xuexi Tie 8/13/2019 12:00 PM

Deleted:

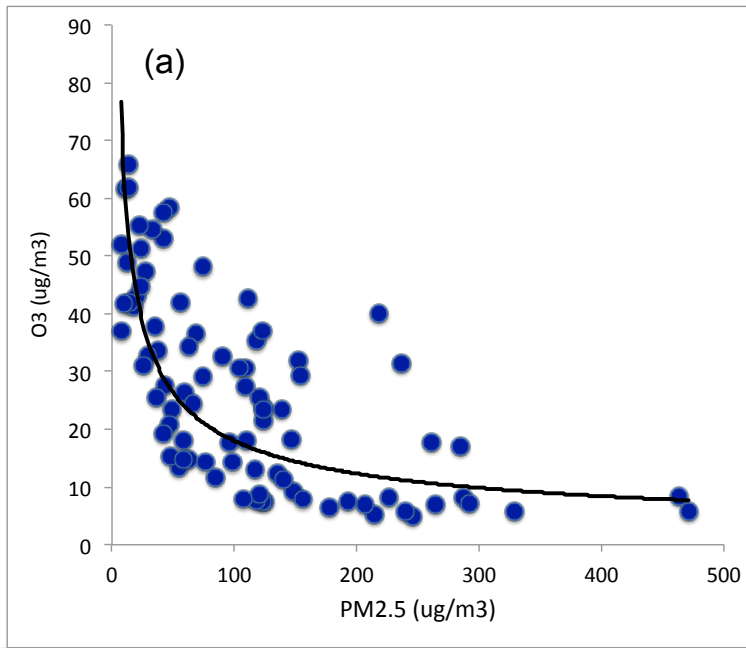
Unknown

Formatted: Font:(Default) Times New Roman

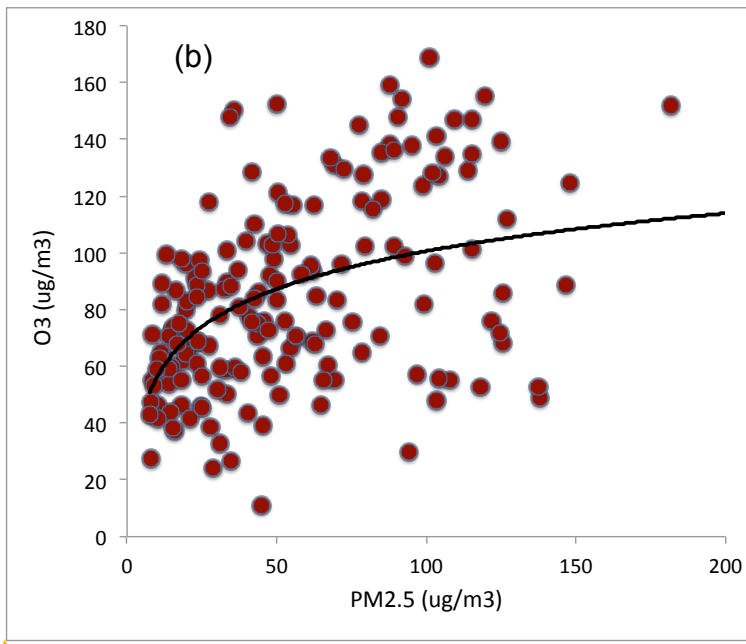
Xuexi Tie 8/13/2019 2:36 PM

Formatted: Font:12 pt

717

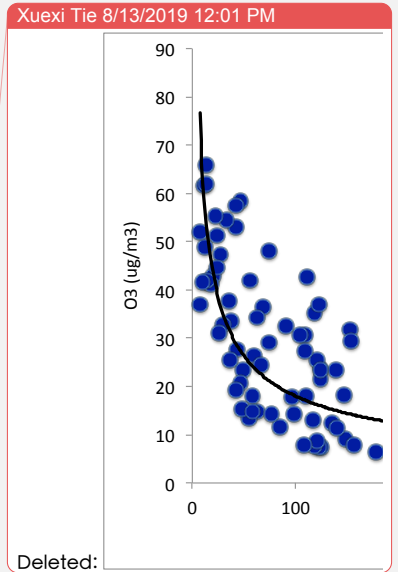


718
719

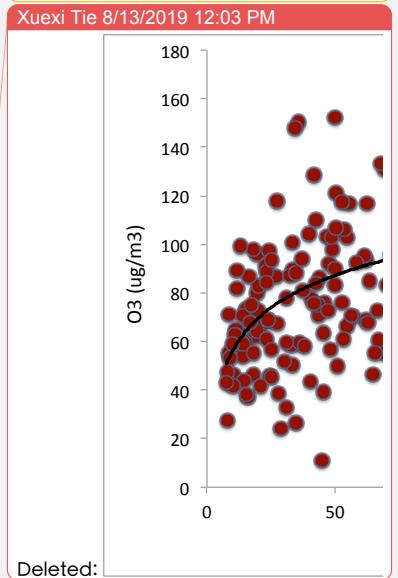


720
721

Fig. 3. The correlation between O_3 and $PM_{2.5}$ concentrations during winter (upper **a**) and from late spring to early fall (panel **b**). During winter, O_3 concentrations were strong anti-correlated with the $PM_{2.5}$ concentrations. From late spring to early fall, O_3 concentrations were correlated with the $PM_{2.5}$ concentrations.



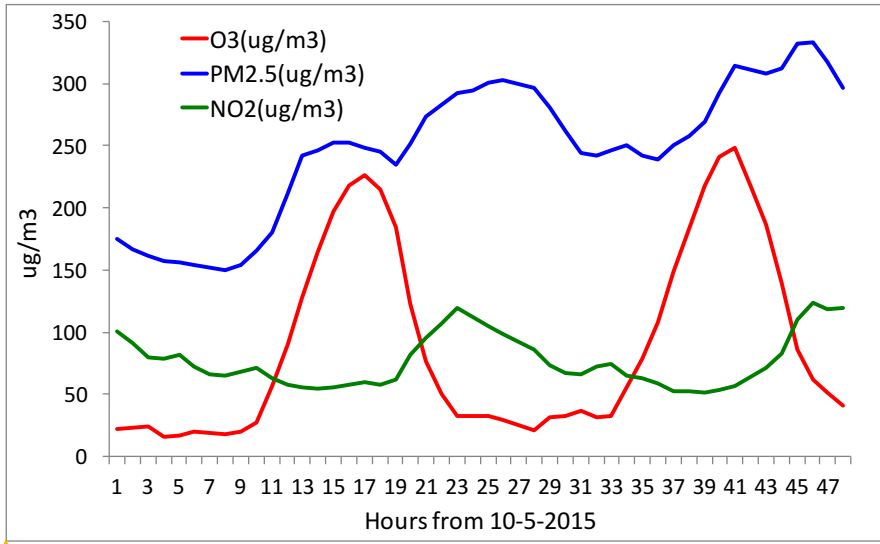
Deleted:
Unknown
Formatted: Font:(Default) Times New Roman



Deleted:
Unknown
Formatted: Font:(Default) Times New Roman

Xuexi Tie 8/13/2019 2:36 PM
Formatted: Font:12 pt
Xuexi Tie 8/13/2019 12:04 PM
Deleted: panel
Xuexi Tie 8/13/2019 12:05 PM
Deleted: lower

730



731
732
733
734
735
736
737

Fig. 4. The diurnal variations of PM_{2.5} (blue line) and O₃ (red line), and NO₂ (green line) during a fall period (from Oct. 5 to Oct. 6, 2015). It shows that with high PM_{2.5} condition, there was a strong O₃ diurnal variation.

Unknown

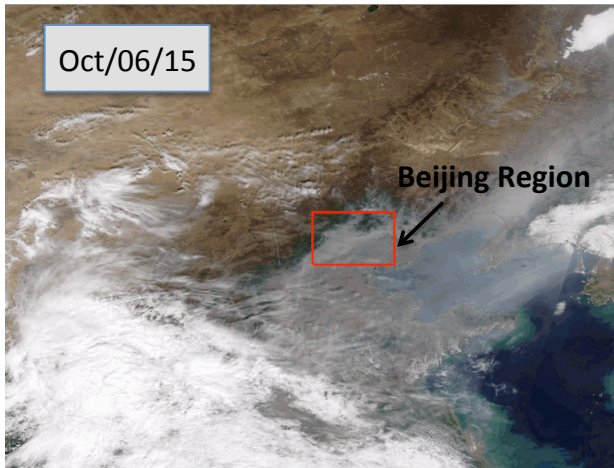
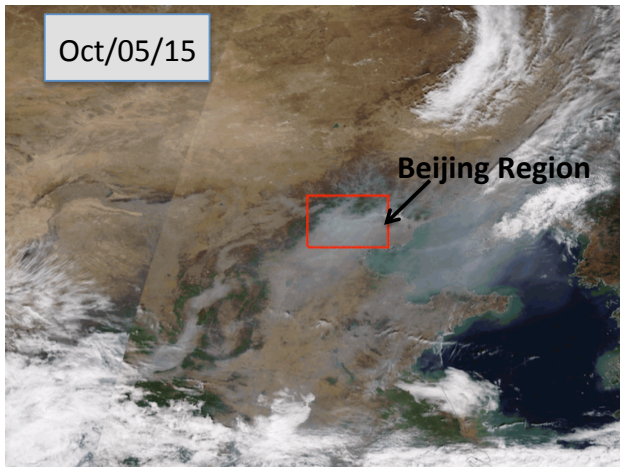
Formatted: Font:(Default) Times New Roman

Xuexi Tie 8/13/2019 12:05 PM

Deleted:

Xuexi Tie 8/13/2019 2:36 PM

Formatted: Font:12 pt



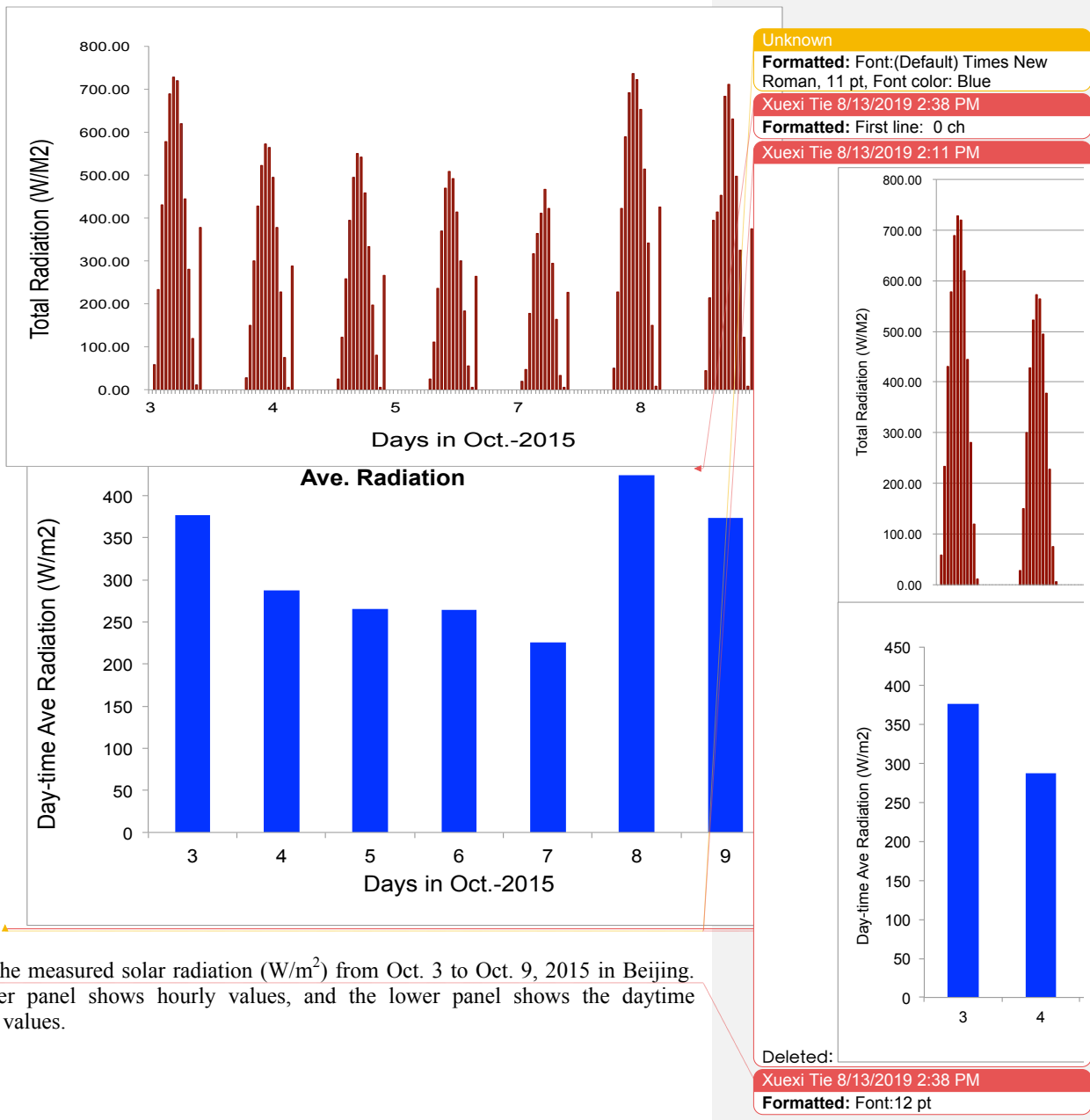
739
740
741
742
743
744
745

Fig. 5. The cloud condition during the period of the case study (between Oct 5 and 6, 2015 in the Beijing region. The bright white color shows the cloud covers, and the grey white shows the haze covers. The Beijing region is under the heavy haze conditions during the period.

Xuexi Tie 8/13/2019 12:06 PM
Formatted: Indent: First line: 4.28 ch

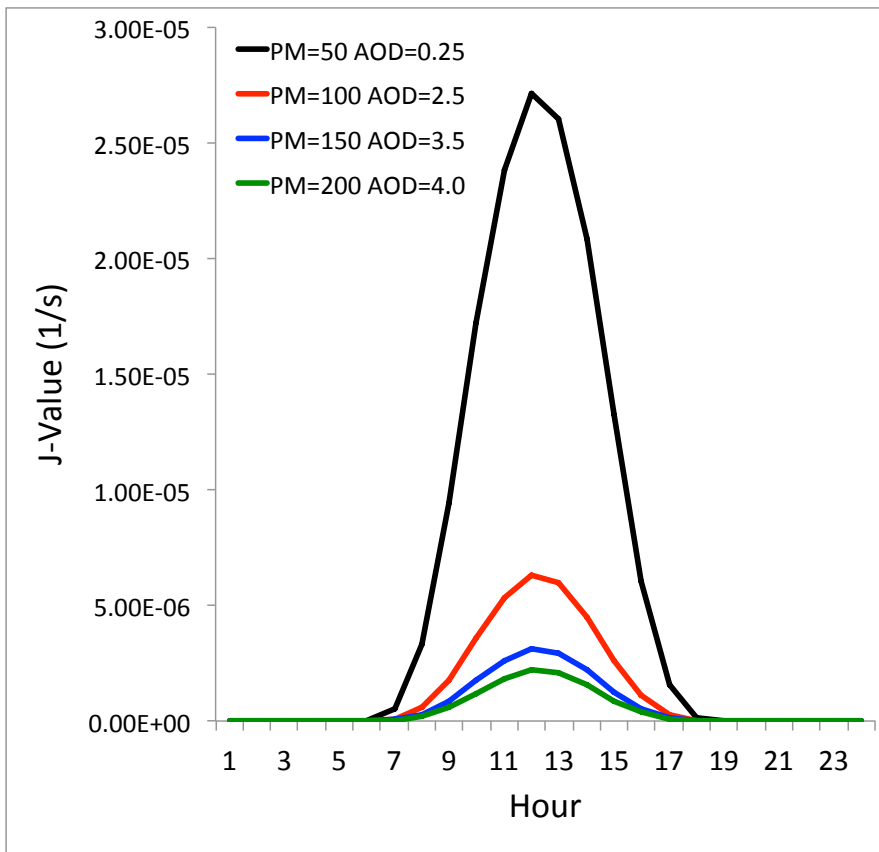
Xuexi Tie 8/13/2019 2:14 PM
Formatted: Indent: First line: 4.28 ch

Xuexi Tie 8/13/2019 2:36 PM
Formatted: Font:12 pt



746
747
748
749
750
751
752

Fig. 6. The measured solar radiation (W/m²) from Oct. 3 to Oct. 9, 2015 in Beijing. The upper panel shows hourly values, and the lower panel shows the daytime averaged values.



754
755
756
757
758
759

Fig. 7. The effect of aerosol levels with AOD = 0.25 (black line), AOD = 2.5 (red line), AOD = 3.5 (blue line), and AOD = 4.0 (green line) on the O₃ photolysis calculated by the TUV model in October at middle-latitude.

Xuexi Tie 8/13/2019 2:13 PM

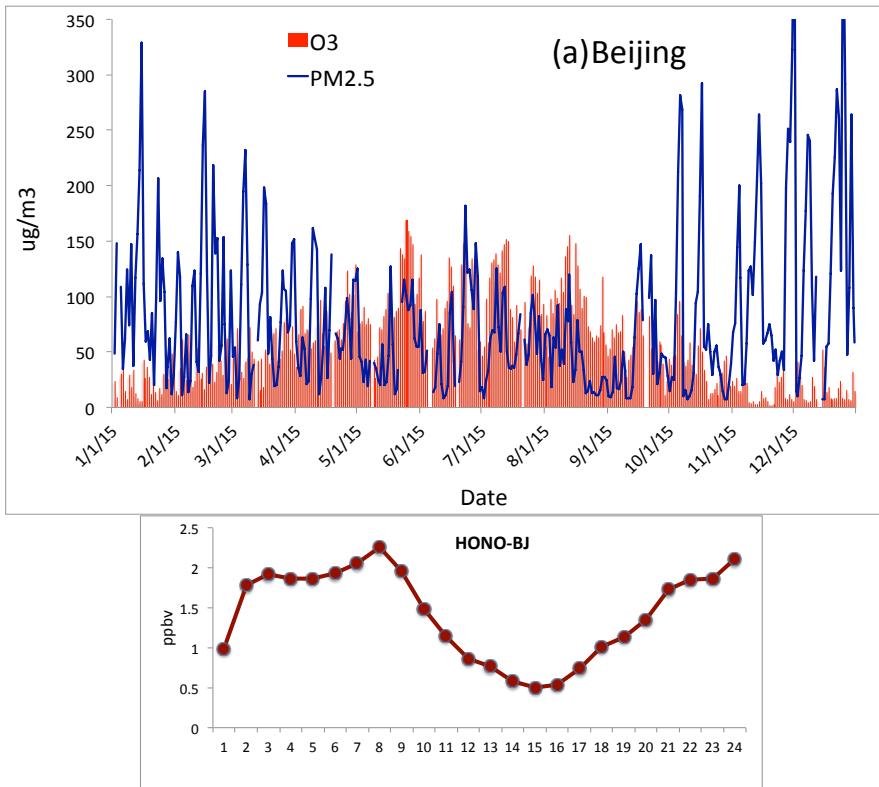
Deleted:

Unknown

Formatted: Font:(Default) Times New Roman, Font color: Text 1

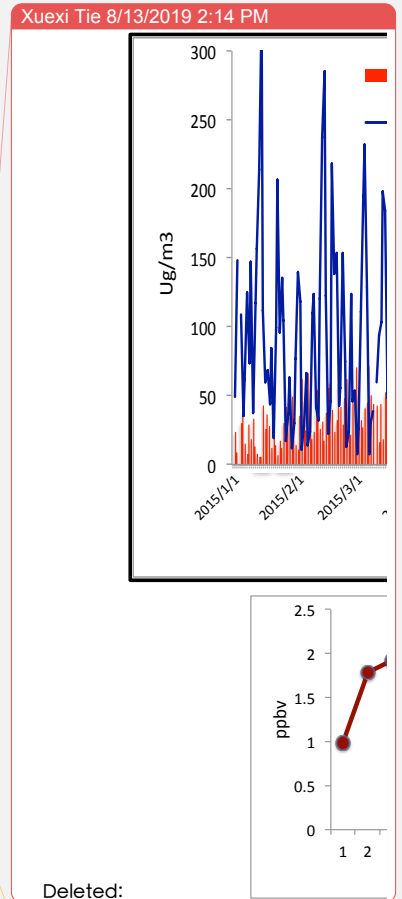
Xuexi Tie 8/13/2019 2:38 PM

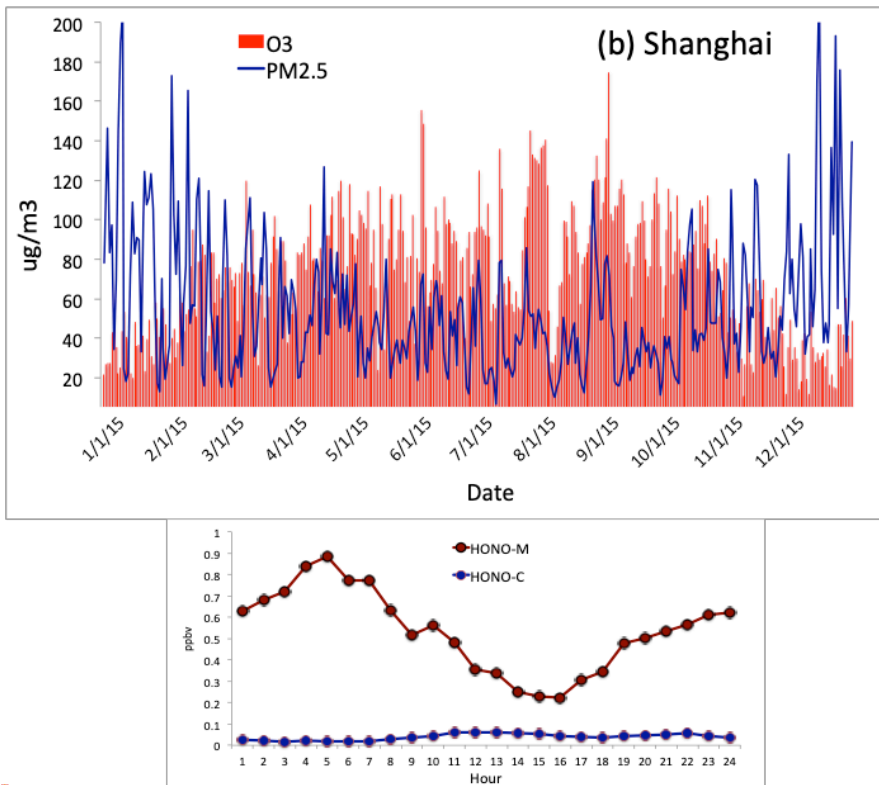
Formatted: Font:12 pt



761
762
763
764
765
766
767
768

Fig. 8a. The measured HONO concentrations (ppbv) and the PM_{2.5} and O₃ daily concentrations in Beijing. The upper panel shows the measured daily concentrations of PM_{2.5} and O₃ as shown in Fig.2. The dark-red line was measured HONO in Beijing from 1 to 27 January, 2014.





770
771
772
773
774
775
776
777
778

Fig. 8b. The measured HONO concentrations (ppbv) and the PM_{2.5} and O₃ daily concentrations in Shanghai. The upper panel shows the measured daily concentrations of PM_{2.5} and O₃ in 2015. The dark-red line was measured in Shanghai from 9 to 18 September, 2009. The green line was calculated by the WRF-Chem model.

Xuexi Tie 8/13/2019 2:15 PM

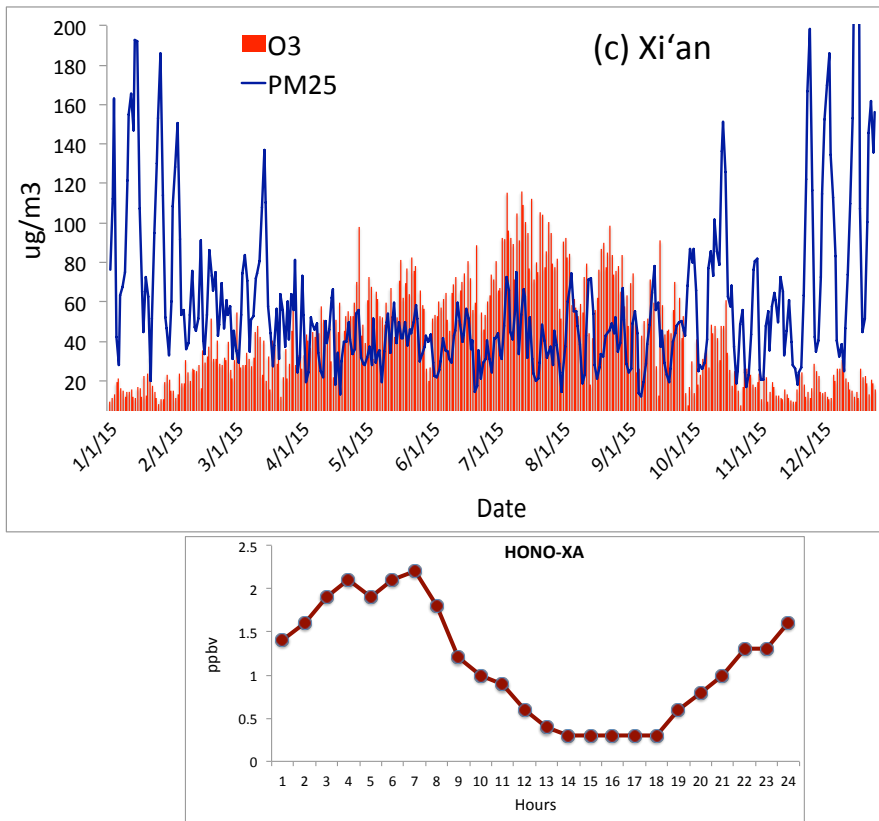
Deleted:

Unknown

Formatted: Font:(Default) Times New Roman, 11 pt, Font color: Text 1

Xuexi Tie 8/13/2019 2:38 PM

Formatted: Font:12 pt



780
781
782
783
784
785
786
787
788
789
790
791

Fig. 8c. The measured HONO concentrations (ppbv) and the PM_{2.5} and O₃ daily concentrations in Xi'an. The upper panel shows the measured daily concentrations of PM_{2.5} and O₃ in 2015. The red line was measured HONO in Xi'an from 24 July to August 6, 2015.

Xuexi Tie 8/13/2019 2:15 PM

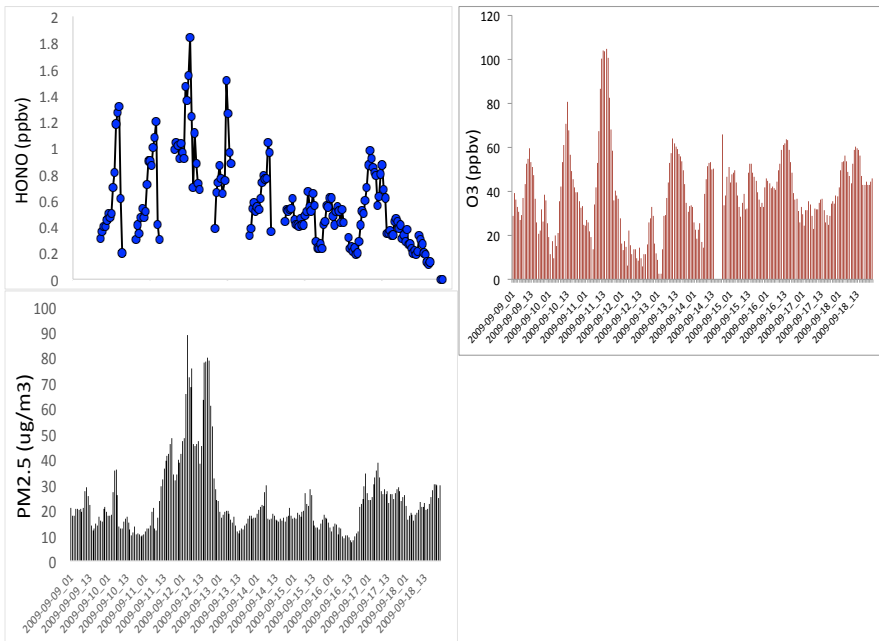
Deleted:

Unknown

Formatted: Font:(Default) Times New Roman, 11 pt, Font color: Text 1

Xuexi Tie 8/13/2019 2:38 PM

Formatted: Font:12 pt



793
794
795
796

Fig. 9. The measured HONO (upper left panel), PM_{2.5} concentrations (lower left panel), and O₃ concentrations (upper right panel) in fall in Shanghai. It illustrates that the high HONO concentrations were corresponded with high PM_{2.5} concentrations.

Xuexi Tie 8/13/2019 2:16 PM

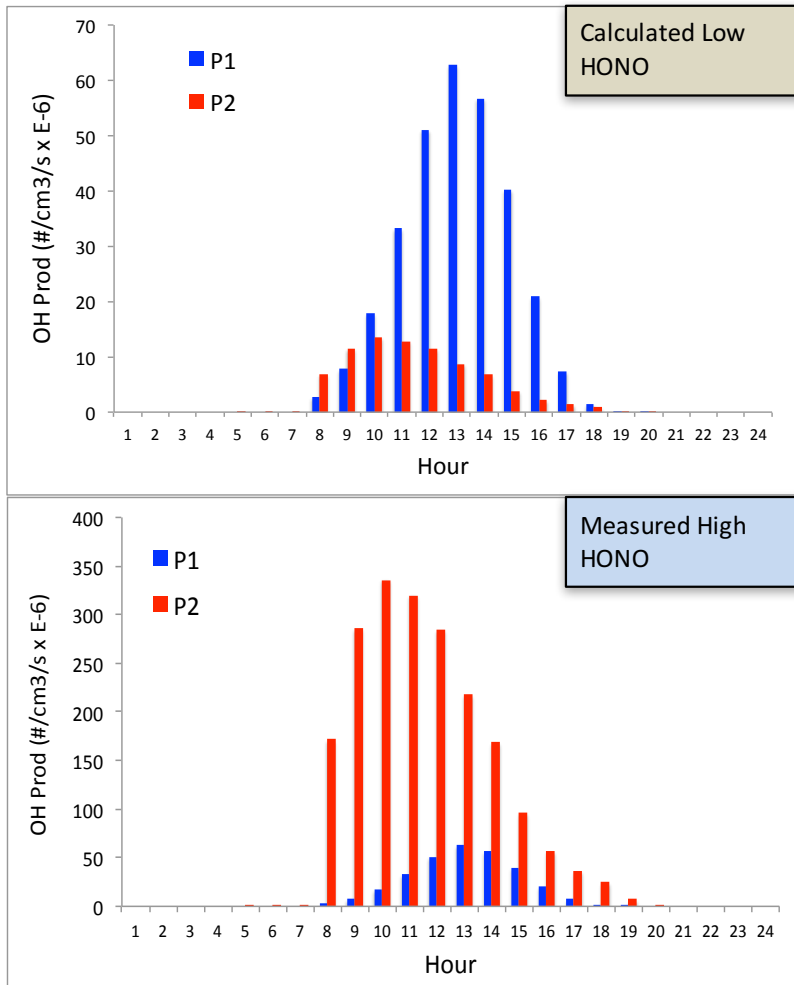
Deleted:

Unknown

Formatted: Font:(Default) Times New Roman, Bold

Xuexi Tie 8/13/2019 2:38 PM

Formatted: Font:12 pt



798
799
800
801
802
803
804

Fig. 10. The calculated OH production P(HOx) ($\#/cm^3/s$) by using the model calculated HONO (low concentrations) (in the upper panel) and by using the measured HONO (high concentrations) (in the lower panel). The red bars represent the calculation of the P1 term, and the red bars represent the calculation of the P2 term (OH production from HONO).

Xuexi Tie 8/13/2019 2:39 PM
Formatted: Font:12 pt

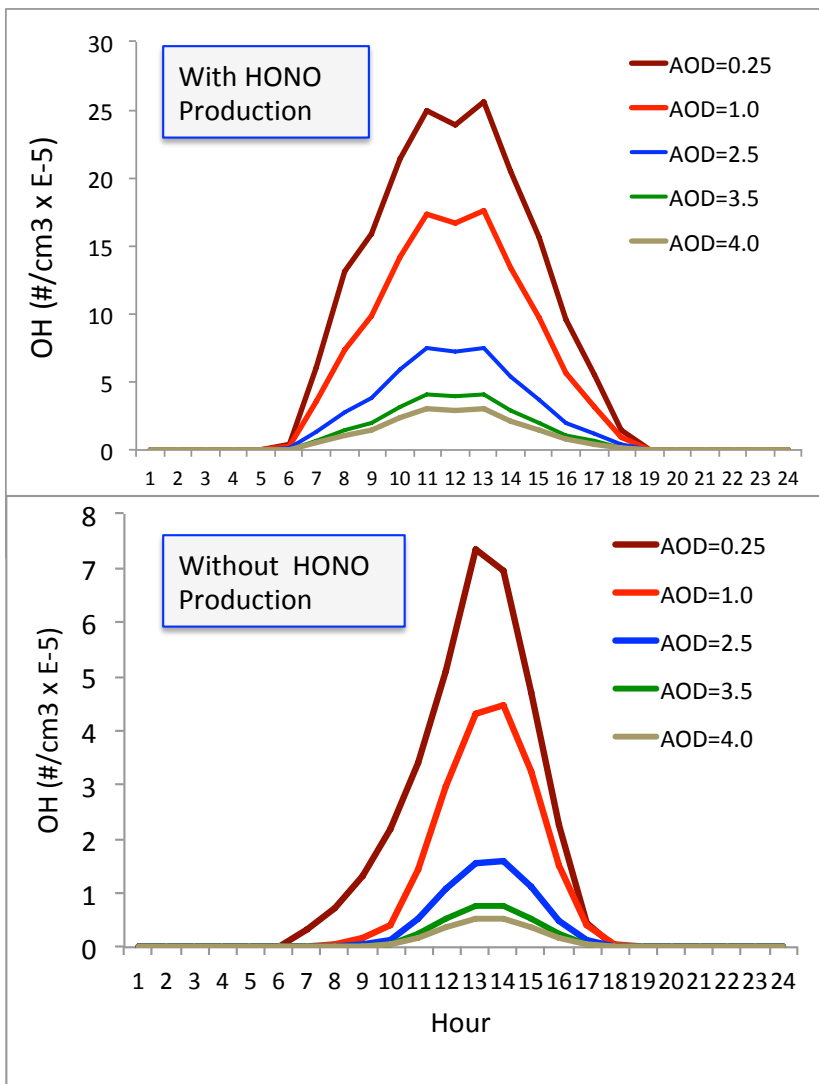
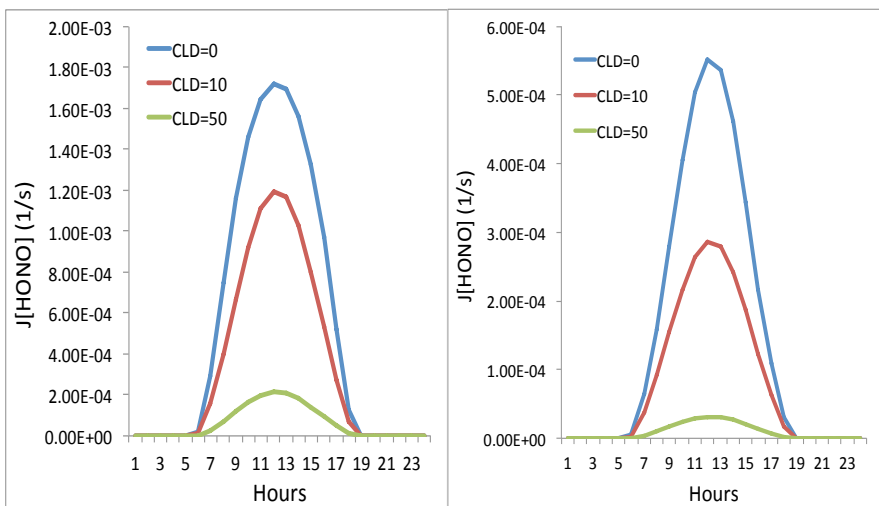


Fig. 11. The calculated OH concentrations ($\#/\text{cm}^3$) with (upper panel) and without (lower panel) HONO production of OH, under different aerosol levels. Dark red (AOD=0.25), red (AOD=2.5), red (AOD=3.5), and red (AOD=4.0).

Xuexi Tie 8/13/2019 2:39 PM
Formatted: Font:12 pt

805
806
807
808
809
810
811
812
813



814
815
816
817
818
819
820
821
822
823
824
825
826

Fig. 12. The effect of cloud cover on the photolysis rate of HONO ($J[\text{HONO}]$). The blue, red, and green lines represent the cloud water vapor of 0 (cloud-free), 10 (g/m^3 – thin cloud), and 50 (g/m^3 – thick cloud), respectively. The left panel represents the light aerosol condition, with AOD of 0.25, and the right panel represents the heavy aerosol condition, with AOD of 2.5.

Xuexi Tie 8/13/2019 2:17 PM

Deleted:

Unknown

Formatted: Font:(Default) Times New Roman

Xuexi Tie 8/13/2019 2:39 PM

Formatted: Font:12 pt

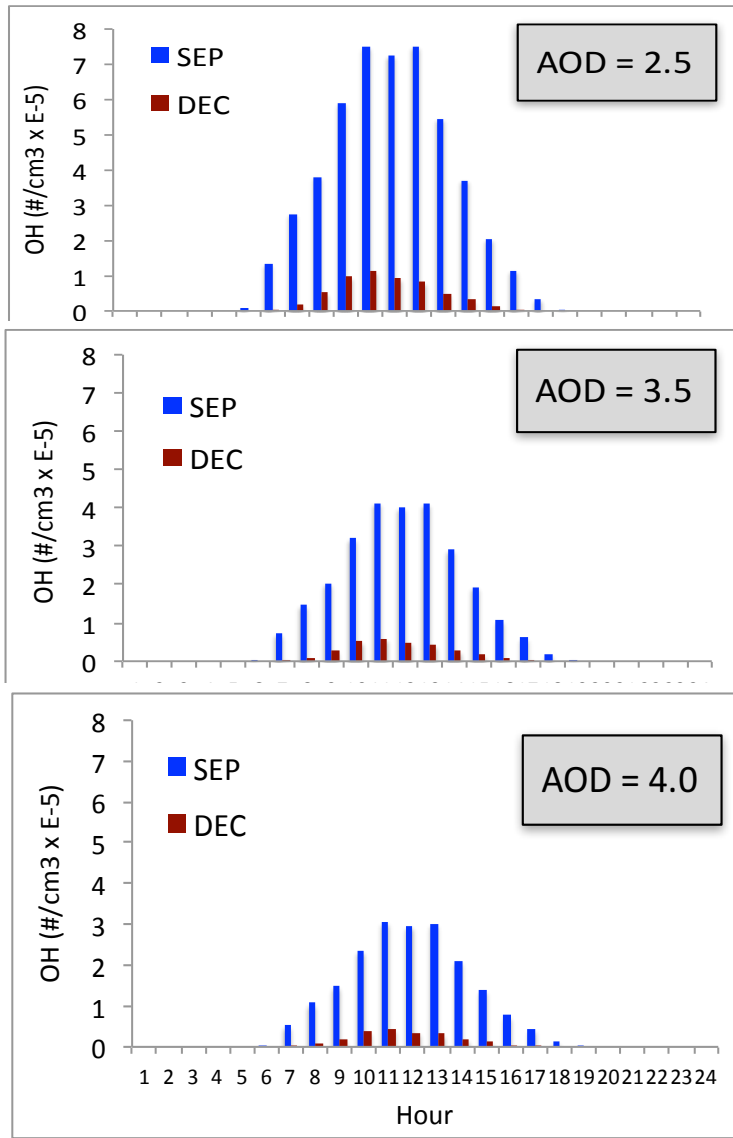
Xuexi Tie 8/13/2019 2:18 PM

Deleted: (A)

Xuexi Tie 8/13/2019 2:18 PM

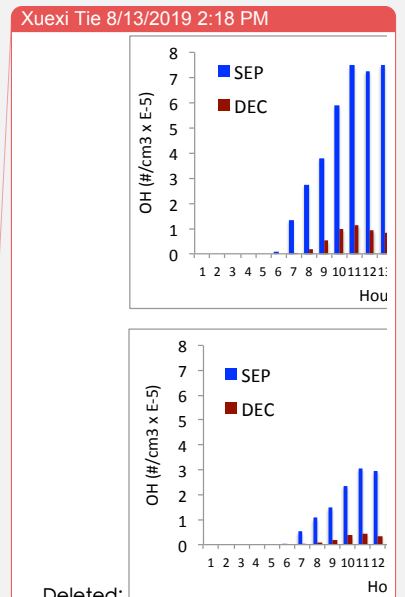
Deleted: (B)

830
831



832
833
834
835
836

Fig. 13. The calculated OH concentrations in September (blue bars) and December (dark red bars), under different aerosol levels.



Unknown
Formatted: Font:(Default) Times New Roman

Xuexi Tie 8/13/2019 2:39 PM
Formatted: Font:12 pt